

## THE OPTX PROJECT III: X-RAY VERSUS OPTICAL SPECTRAL TYPE FOR AGNS<sup>1</sup>

L. TROUILLE<sup>2</sup>, A. J. BARGER<sup>2,3,4</sup>, L. L. COWIE<sup>4</sup>, Y. YANG<sup>5</sup>, AND R. F. MUSHOTZKY<sup>6</sup>

*Draft version November 2, 2018*

### ABSTRACT

We compare the optical spectral types with the X-ray spectral properties for a uniformly selected (sources with fluxes greater than the  $3\sigma$  level and above a flux limit of  $f_{2-8\text{ keV}} > 3.5 \times 10^{-15} \text{ erg cm}^{-2} \text{ s}^{-1}$ ), highly spectroscopically complete ( $> 80\%$  for  $f_{2-8\text{ keV}} > 10^{-14} \text{ erg cm}^{-2} \text{ s}^{-1}$  and  $> 60\%$  below)  $2-8\text{ keV}$  X-ray sample observed in three *Chandra* fields (CLANS, CLASXS, and the CDF-N) that cover  $\sim 1.2 \text{ deg}^2$ . For our sample of 645 spectroscopically observed sources, we confirm that there is significant overlap of the X-ray spectral properties, as determined by the effective photon indices,  $\Gamma_{\text{eff}}$ , obtained from the ratios of the  $0.5-2\text{ keV}$  to  $2-8\text{ keV}$  counts, for the different optical spectral types. For example, of the broad-line AGNs (non-broad-line AGNs),  $20\% \pm 3\%$  ( $33\% \pm 4\%$ ) have  $\Gamma_{\text{eff}} < 1.2$  ( $\Gamma_{\text{eff}} \geq 1.2$ ). Thus, one cannot use the X-ray spectral classifications and the optical spectral classifications equivalently. Since it is not understood how X-ray and optical classifications relate to the obscuration of the central engine, we strongly advise against a mixed classification scheme, as it can only complicate the interpretation of X-ray AGN samples. We confirm the dependence of optical spectral type on X-ray luminosity, and for  $z < 1$ , we find a similar luminosity dependence of  $\Gamma_{\text{eff}}$ . However, this dependence breaks down at higher redshifts due to the highly redshift-dependent nature of  $\Gamma_{\text{eff}}$ . We therefore also caution that any classification scheme which depends on  $\Gamma_{\text{eff}}$  is likely to suffer from serious redshift bias.

*Subject headings:* cosmology: observations — galaxies: active

### 1. INTRODUCTION

Starting with the first *Chandra* observations which resolved the X-ray background (Mushotzky et al. 2000), ultradeep, small-area (2 Ms CDF-N, Brandt et al. 2001, Alexander et al. 2003; 2 Ms CDF-S, Giacconi et al. 2002, Luo et al. 2008) and intermediate-depth, wider-area (SEXSI, Harrison et al. 2003; CLASXS, Yang et al. 2004; AEGIS-X, Nandra et al. 2005, Laird et al. 2009; extended-CDF-S or eCDF-S, Lehmer et al. 2005, Virani et al. 2006; ChaMP, Kim et al. 2007; CLANS, Trouille et al. 2008; COSMOS, Elvis et al. 2009) *Chandra* X-ray surveys have uncovered a substantial population of active galactic nuclei (AGNs) that were not previously identified in optical or soft X-ray surveys, revolutionizing our understanding of accretion onto supermassive black holes. Spectroscopic follow-up is essential for tracing the evolution of X-ray-selected AGNs over cosmic time, and over the years a large number of redshifts have been obtained for all of the above fields. However, the CDF-N (Hornschemeier et al. 2001; Barger et al. 2002; Barger et al. 2003; Trouille et al. 2008), 1 Ms CDF-S (Szokoly

et al. 2004), CLASXS (Steffen et al. 2004; Trouille et al. 2008), and CLANS (Trouille et al. 2008) fields are the most uniformly spectroscopically complete of all of the *Chandra* surveys to date, and the high-quality spectral data in these fields can be used to classify the sources optically. (See Table 1 in Trouille et al. 2008 for a summary of the spectroscopic completeness of the eCDF-S, AEGIS-X, SEXSI, and ChaMP fields and Figure 3 in this paper for the combined completeness of our CDF-N, CLASXS, and CLANS fields.)

This is the third paper in our OPTX series, which focuses on the analysis of the X-ray sources in the CDF-N, CLASXS, and CLANS fields. In the first paper (Trouille et al. 2008) we presented a new X-ray catalog for the CLANS field, as well as new (CLANS) and updated (CLASXS, CDF-N) redshift catalogs for the three fields. In the second paper (Yenko et al. 2009) we constructed rest-frame hard X-ray luminosity functions using our three fields, the CDF-S, an ASCA survey (Akiyama et al. 2000), and the local SWIFT 9-month Burst Alert Telescope (BAT) survey (Tueller et al. 2008; Winter et al. 2008, 2009). Since it is very important to have a physically motivated classification scheme for understanding AGN evolution, in this paper we use our high-quality Deep Imaging Multi-Object Spectrograph (DEIMOS; Faber et al. 2003) data from Keck II to explore the differences between the optical, X-ray, and mixed classification schemes that have been proposed for analyzing *Chandra* X-ray samples.

As two different groups began carrying out extensive spectroscopy of the ultradeep CDFs and releasing the measurements to the public, it became clear that a consistent optical classification system for these faint X-ray sources was needed so that the data could be analyzed together. Szokoly et al. (2004) and Barger et al. (2005)

<sup>1</sup> Some of the data presented herein were obtained at the W. M. Keck Observatory, which is operated as a scientific partnership among the California Institute of Technology, the University of California, and the National Aeronautics and Space Administration. The observatory was made possible by the generous financial support of the W. M. Keck Foundation.

<sup>2</sup> Department of Astronomy, University of Wisconsin-Madison, 475 N. Charter Street, Madison, WI 53706

<sup>3</sup> Department of Physics and Astronomy, University of Hawaii, 2505 Correa Road, Honolulu, HI 96822

<sup>4</sup> Institute for Astronomy, University of Hawaii, 2680 Woodlawn Drive, Honolulu, HI 96822

<sup>5</sup> Department of Astronomy, University of Illinois, 1002 W. Green St., Urbana, IL 61801

<sup>6</sup> NASA Goddard Space Flight Center, Code 662, Greenbelt, MD 20771

pointed out that it would be problematic to apply classical optical AGN definitions to the faint X-ray sources due to the range of rest-frame wavelengths covered and the varying degree of mixing of the AGN spectrum with the host galaxy spectrum at different redshifts. Moreover, by this time it was already well known that many luminous X-ray sources showed no signatures of AGN activity in their optical spectra (e.g., Barger et al. 2001; Hornschemeier et al. 2001). Thus, Szokoly et al. (2004) proposed a new optical classification scheme, which Barger et al. (2005) roughly matched by defining the following spectral types: (1) absorbers (ABS; no strong emission lines); (2) star formers (SF; strong Balmer lines and no broad or high-ionization lines); (3) high-excitation sources (HEX; [NeV], CIV, narrow MgII lines, or strong [OIII]); and (4) broad-line AGNs (BLAGNs; optical lines having FWHM line widths  $> 2000 \text{ km s}^{-1}$ ). Although the HEX spectral type largely overlaps the classical Seyfert 2 spectral type, describing the sources as HEX sources helps to avoid confusion with the classical definitions.

X-ray data alone have also long been used to estimate the amount of obscuration between the observer and the nuclear source through the  $0.5 - 8 \text{ keV}$  spectral slope. Since  $2 - 8 \text{ keV}$  X-rays will penetrate obscuring material (except in Compton-thick AGNs, where the neutral hydrogen column density,  $N_{\text{H}}$ , in the line of sight is higher than the inverse Thomson cross section,  $N_{\text{H}} \simeq 1.5 \times 10^{24} \text{ cm}^{-2}$ ) and  $0.5 - 2 \text{ keV}$  X-rays will not, in low signal-to-noise data a shallower slope may indicate an obscured source. X-ray spectra can be approximated with a power-law of the form  $P(E) = AE^{-\Gamma_{\text{eff}}}$ , where  $E$  is the photon energy in keV and  $A$  is the normalization factor. (Here we indicate the power law slope as an *effective*  $\Gamma$  to distinguish it from the intrinsic slope,  $\Gamma$ .  $\Gamma_{\text{eff}}$  is not the true  $\Gamma$  unless there is no intrinsic absorption.) Barger et al. (2005) showed that Szokoly et al. (2004)'s choice of  $2000 \text{ km s}^{-1}$  as the dividing line between BLAGNs and non-BLAGNs in the optical classification scheme made sense in terms of the X-ray spectral properties, as above  $2000 \text{ km s}^{-1}$  almost all of the sources are X-ray soft ( $\Gamma_{\text{eff}} = 1.8$ ), whereas below this line width there is a wide span of X-ray colors.

In addition to their optical classification scheme, Szokoly et al. (2004) introduced a classification scheme that follows the unified model for AGNs (Antonucci 1993) and is based solely on the X-ray properties of the sources. In this scheme objects with unabsorbed X-ray luminosities stronger than expected from stellar processes in normal galaxies (i.e.,  $L_{0.5-10 \text{ keV}} \geq 10^{42} \text{ erg s}^{-1}$ ) are classified as AGNs, and unabsorbed sources are separated from absorbed sources through the use of a *Chandra*-specific X-ray hardness ratio,  $\text{HR} = (C_{\text{hard}} - C_{\text{soft}}) / (C_{\text{hard}} + C_{\text{soft}})$ , where  $C_{\text{hard}}$  and  $C_{\text{soft}}$  are the net ACIS-I count rates in the hard ( $2 - 10 \text{ keV}$ ) and soft ( $0.5 - 2 \text{ keV}$ ) bands, respectively. They chose  $\text{HR} \leq -0.2$  to indicate an unabsorbed source (which they call an X-ray type 1 source) and  $\text{HR} > -0.2$  to indicate an absorbed source (which they call an X-ray type 2 source). (Note that this HR is approximately equivalent to, at  $z = 0$ , our  $\Gamma_{\text{eff}} = 1.2$ .) However, they noted that while an increasing absorption makes a source harder, a higher redshift makes a source softer

(the  $2 - 10 \text{ keV}$  filter samples higher energies which are less affected by obscuring material), which means this approach might incorrectly identify a high-redshift absorbed (X-ray type 2) source as an unabsorbed (X-ray type 1) source.

Hasinger et al. (2005) took the classification of X-ray sources one step further, arguing for a third scheme that is a mix of the above two schemes. This decision was based on their assumption that ‘true’ BLAGNs may be optically misclassified as non-BLAGNs due to dilution of the AGN light by the host galaxy light, particularly at lower luminosities (Moran et al. 2002; Severgnini et al. 2003; Garcet et al. 2007; Cardamone et al. 2007). Thus, according to Hasinger et al. (2005), the most ‘complete’ sample of unobscured AGNs is one which includes any object optically classified as a BLAGN, as well as any object satisfying  $L_{0.5-10 \text{ keV}} \geq 10^{42} \text{ erg s}^{-1}$  and  $\text{HR} \leq -0.2$ .

Unfortunately, the creation of a classification scheme that mixes optical and X-ray spectral diagnostics requires a thorough understanding of the correspondence between X-ray and optical spectral type. However, it is well known observationally (yet unexplained physically) that  $\sim 10 - 30\%$  of AGNs have (1) X-ray spectra that show no absorption and (2) optical spectra that suggest obscuration (e.g., Pappa et al. 2001; Panessa & Bassani 2002; Barcons et al. 2003; Georgantopoulos & Zezas 2003; Caccianiga et al. 2004; Corral et al. 2005; Wolter et al. 2005; Mateos et al. 2005; Tozzi et al. 2006). The opposite effect, i.e., (1) X-ray spectra that show absorption and (2) optical spectra that suggest no obscuration, has also been observed (e.g., Silverman et al. 2005 found that  $\sim 15\%$  of X-ray hard AGNs in ChAMP are BLAGNs; other examples can be found in Comastri et al. 2001; Wilkes et al. 2002; Fiore et al. 2003; Brusa et al. 2003; Akiyama et al. 2003; Silverman et al. 2005; Gallagher et al. 2006; Hall et al. 2006; Tajer et al. 2007).

Moreover, the assumption that galaxy dilution is causing BLAGNs to be optically misclassified as non-BLAGNs has been called into question by two studies. Barger et al. (2005) used the *Hubble Space Telescope* Great Observatories Origins Deep Survey North (GOODS-N; Giavalisco et al. 2004) data to measure the nuclear UV magnitudes of AGNs in the CDF-N. It is well known that the nuclear UV magnitudes of BLAGNs are strongly correlated with the  $0.5 - 2 \text{ keV}$  fluxes (e.g., Zamorani et al. 1981), and, indeed Barger et al. (2005) found that their BLAGNs also showed this correlation. However, they also found that the non-BLAGNs in their sample did not; rather, the UV nuclei of these sources were much weaker relative to their X-ray light than would be expected if they were similar to the BLAGNs. In the second study, Cowie et al. (2009) combined Galaxy Evolution Explorer (GALEX; Martin et al. 2005) data with the CDF-N, CLASXS, and CLANS X-ray samples to determine the ionizing flux from  $z \sim 1$  AGNs. They found that while the BLAGNs in their sample exhibited substantial UV ionizing flux, the non-BLAGNs were UV faint.

Here we use our extensive observations of the CDF-N, CLASXS, and CLANS fields to analyze the optical and X-ray spectral properties of a significant (fluxes  $> 3\sigma$  level), intermediate-depth ( $f_{2-8 \text{ keV}} > 3.5 \times$

TABLE 1  
CLANS, CLASXS, AND CDF-N SURVEY CHARACTERISTICS

	CLANS	CLASXS	CDF-N
Total Exposure	70 ks	40 ks (70 ks <sup>b</sup> )	2 Ms
Area (deg <sup>2</sup> )	0.6	0.45	0.124
2 – 8 keV flux limit <sup>a</sup>	35	60 (35 <sup>b</sup> )	1.4

<sup>a</sup> $10^{-16}$  erg cm<sup>-2</sup> s<sup>-1</sup>;  $3 \sigma$  flux limit at the pointing center, see Trouille et al. (2008).

<sup>b</sup>The central CLASXS pointing.

$10^{-15}$  erg cm<sup>-2</sup> s<sup>-1</sup>) sample of X-ray sources. Due to the need for a large and very complete optical spectroscopic sample, this is the first time that such a comparative study has been done. Of particular interest is the relationship between the X-ray spectral properties and the optical spectral properties of X-ray-selected sources and whether such characteristics map each other well enough that they can be merged into a single classification scheme.

The structure of the paper is as follows. In Section 2 we describe our X-ray samples. In Section 3 we discuss our spectroscopic completeness and optical classifications and show the redshift distributions by optical spectral type. In Section 4 we compare our optical classifications with the X-ray classifications, and we illustrate the challenges of a mixed classification scheme. In Section 5 we examine in the context of our data the observational obstacles that have been invoked to explain the observed mismatches between X-ray and optical spectral types, and in Section 6 we present our conclusions.

All magnitudes are in the Vega magnitude system. We assume  $\Omega_M = 0.3$ ,  $\Omega_\Lambda = 0.7$ , and  $H_0 = 70$  km s<sup>-1</sup> Mpc<sup>-1</sup> throughout.

## 2. X-RAY DATA

We construct our 2 – 8 keV sample from three different fields in the sky, so known field-to-field variations due to large scale structure are minimized. All three of our fields sample regions of low Galactic HI column density. Both the CLANS and CLASXS fields reside in the Lockman Hole high-latitude region of extremely low Galactic HI column density ( $5.7 \times 10^{19}$  cm<sup>-2</sup>; Lockman et al. 1986). The Galactic HI column density along the line of sight to the CDF-N is  $1.6 \times 10^{20}$  cm<sup>-2</sup> (Stark et al. 1992).

In Table 1 we list the *Chandra* exposure times, the areas covered, and the 2 – 8 keV  $3 \sigma$  flux limits at the pointing centers. Because the CLANS and CLASXS fields are shallower than the CDF-N field, we have limited our study to sources with fluxes greater than the  $3 \sigma$  flux limit at the pointing center of the 70 ks CLANS pointings (i.e.,  $f_{2-8 \text{ keV}} > 3.5 \times 10^{-15}$  erg cm<sup>-2</sup> s<sup>-1</sup>). We note that although only the central CLASXS pointing is  $\sim 70$  ks (the other eight are 40 ks), the CLASXS survey was designed to achieve uniform field coverage, and so there is substantial overlap between pointings. Also, since our goal is simply to create a uniform sample of sources above a given flux limit for the purposes of studying their X-ray and optical spectral characteristics, the choice of flux limit will not greatly affect our present results (as opposed to, for example, the impact it would have on determining the number densities).

To construct a significant 2 – 8 keV sample, we additionally only use sources with fluxes greater than the  $3 \sigma$  level. We determined this by using the  $1 \sigma$  error

bars on the 2 – 8 keV fluxes given in Alexander et al. (2003), Yang et al. (2004), and Trouille et al. (2008) for the CDF-N, CLASXS, and CLANS fields, respectively. Hereafter, this paper’s “2 – 8 keV sample” consists of 745 X-ray sources selected in the 2 – 8 keV band.

## 3. CLASSIFICATION BY OPTICAL SPECTRAL TYPE

Trouille et al. (2008) present the details of our spectroscopic observations of the X-ray sources in the CLANS, CLASXS, and CDF-N fields, including how the observations were made, the data reduction process, and the latest redshift catalogs.

We provide a catalog of updated values for the CLANS field in Table 2. We ordered the sources by increasing right ascension and labeled each with the same source number (col [1]) as in Trouille et al. (2008). CLANS #761 through #789 were inadvertently not included in the original Trouille et al. (2008) CLANS catalog, and so are included here. CLANS #80, #150, and #404 in the Trouille et al. (2008) catalog had incorrect 2 – 8 keV fluxes as a result of their anomalously high hardness ratio values. Here we list their corrected fluxes determined using the HEASARC WebPIMMS tool and assuming  $\Gamma = 1.4$ . The remaining sources are included as a result of our spectroscopic observations with DEIMOS on Keck II in Spring 2009.

Columns (2) and (3) give the right ascension and declination coordinates. Columns (4) and (5) list the net counts in the 0.5 – 2 keV and 2 – 8 keV bands. Columns (6), (7), and (8) provide the X-ray fluxes in the 0.5 – 2 keV, 2 – 8 keV, and 0.5 – 8 keV bands, respectively, in units of  $10^{-15}$  erg cm<sup>-2</sup> s<sup>-1</sup>. The errors quoted are the  $1 \sigma$  Poisson errors, using the approximations from Gehrels (1986). The flux errors do not include the uncertainty in the flux conversion factor; however, the errors are generally dominated by the Poisson errors. Column (9) gives the spectroscopic redshifts and column (10) gives the optical spectral classifications.

For  $f_{2-8 \text{ keV}} > 1.4 \times 10^{-14}$  erg cm<sup>-2</sup> s<sup>-1</sup> (the break flux in the 2 – 8 keV number counts; see Trouille et al. 2008), we have spectroscopic redshifts for 177 of the 208 sources in our 2 – 8 keV sample. We classified our spectroscopically identified sources into the four optical spectral types given in the Introduction. We list the number of sources of each spectral type by field in Table 3. The percentages refer to the percent of identified sources having that spectral type.

In Figure 1 we show the flux distributions by field and all together for the BLAGNs (black), the non-BLAGNs (shaded), the spectroscopically observed but unidentified sources (hatched), and the spectroscopically unobserved sources (open) in our 2 – 8 keV sample. The higher spectroscopic completeness at bright X-ray fluxes is partly due to the fact that at these fluxes the sample is dominated by BLAGNs, which are straightforward to identify. In addition, at fainter X-ray fluxes the sources tend to be optically fainter, making the redshift identifications at these fluxes more difficult. In particular, the intermediate-flux, optically normal galaxies at  $z \sim 2$  are the most difficult to identify spectroscopically.

In Figure 2 we show  $R$  magnitude versus X-ray flux for our 2 – 8 keV sample. AGNs typically lie in the region defined by the loci  $\log(f_X/f_R) = \pm 1$  (e.g., Maccacaro et al. 1988; Schmidt et al. 1998; Hornschemeier et al. 2001;

TABLE 2  
CLANS CATALOG, UPDATED SOURCES

Num. (1)	$\alpha_{2000}$ (2)	$\delta_{2000}$ (3)	$n_{0.5-2 \text{ keV}}$ (4)	$n_{2-8 \text{ keV}}$ (5)	$f_{0.5-2 \text{ keV}}^a$ (6)	$f_{2-8 \text{ keV}}^a$ (7)	$f_{0.5-8 \text{ keV}}^a$ (8)	$z_{spec}$ (9)	class (10)
80	160.8983	58.9781	0.00 <sup>+1.83</sup> <sub>-0.00</sub>	8.25 <sup>+3.69</sup> <sub>-3.03</sub>	0.00 <sup>+0.03</sup> <sub>-0.00</sub>	2.10 <sup>+39.51</sup> <sub>-32.50</sub>	2.03 <sup>+1.01</sup> <sub>-1.01</sub>	1.30	1
150	161.0324	58.6700	0.00 <sup>+1.83</sup> <sub>-0.00</sub>	12.57 <sup>+5.12</sup> <sub>-3.14</sub>	0.00 <sup>+0.03</sup> <sub>-0.00</sub>	2.70 <sup>+29.88</sup> <sub>-29.88</sub>	2.22 <sup>+1.11</sup> <sub>-1.11</sub>	0.00	-99
163	161.0519	58.5388	70.75 <sup>+9.71</sup> <sub>-8.16</sub>	37.75 <sup>+7.47</sup> <sub>-5.89</sub>	7.11 <sup>+0.98</sup> <sub>-0.82</sub>	15.90 <sup>+3.14</sup> <sub>-2.48</sub>	23.00 <sup>+2.52</sup> <sub>-2.18</sub>	0.97	3
380	161.4857	58.9907	4.00 <sup>+3.15</sup> <sub>-1.94</sub>	5.75 <sup>+3.83</sup> <sub>-2.15</sub>	0.34 <sup>+0.27</sup> <sub>-0.17</sub>	2.57 <sup>+1.71</sup> <sub>-0.96</sub>	1.82 <sup>+0.97</sup> <sub>-0.77</sub>	1.10	1
381	161.4875	59.0001	15.00 <sup>+4.95</sup> <sub>-3.84</sub>	5.50 <sup>+4.08</sup> <sub>-1.90</sub>	2.61 <sup>+0.86</sup> <sub>-0.67</sub>	3.35 <sup>+2.49</sup> <sub>-1.16</sub>	6.43 <sup>+1.78</sup> <sub>-1.30</sub>	3.38	3
390	161.5037	59.1229	68.75 <sup>+9.59</sup> <sub>-8.04</sub>	35.75 <sup>+7.30</sup> <sub>-5.73</sub>	6.81 <sup>+0.95</sup> <sub>-0.80</sub>	14.51 <sup>+2.96</sup> <sub>-2.33</sub>	21.02 <sup>+2.42</sup> <sub>-2.00</sub>	1.22	3
404	161.5408	58.9262	0.00 <sup>+1.83</sup> <sub>-0.00</sub>	43.25 <sup>+7.36</sup> <sub>-6.79</sub>	0.00 <sup>+0.02</sup> <sub>-0.00</sub>	9.90 <sup>+102.34</sup> <sub>-94.45</sub>	8.02 <sup>+4.01</sup> <sub>-4.01</sub>	0.29	2
426	161.5699	58.6507	40.00 <sup>+7.37</sup> <sub>-6.30</sub>	19.50 <sup>+4.93</sup> <sub>-4.83</sub>	4.22 <sup>+0.78</sup> <sub>-0.67</sub>	8.32 <sup>+2.10</sup> <sub>-2.06</sub>	13.01 <sup>+1.84</sup> <sub>-1.72</sub>	0.68	2
431	161.5748	58.6362	84.50 <sup>+10.75</sup> <sub>-8.71</sub>	51.50 <sup>+8.75</sup> <sub>-6.69</sub>	7.61 <sup>+0.97</sup> <sub>-0.78</sub>	20.04 <sup>+3.41</sup> <sub>-2.61</sub>	27.92 <sup>+2.57</sup> <sub>-2.46</sub>	0.39	4
440	161.5923	58.6561	25.50 <sup>+6.66</sup> <sub>-4.57</sub>	13.25 <sup>+4.44</sup> <sub>-3.82</sub>	2.78 <sup>+0.50</sup> <sub>-0.50</sub>	5.56 <sup>+1.86</sup> <sub>-1.60</sub>	8.53 <sup>+1.53</sup> <sub>-1.41</sub>	0.95	3
441	161.5930	58.7007	11.00 <sup>+4.41</sup> <sub>-3.28</sub>	23.75 <sup>+6.21</sup> <sub>-4.62</sub>	0.84 <sup>+0.34</sup> <sub>-0.25</sub>	10.81 <sup>+2.83</sup> <sub>-2.10</sub>	8.77 <sup>+2.18</sup> <sub>-1.52</sub>	0.98	1
464	161.6507	58.6700	14.00 <sup>+4.83</sup> <sub>-3.71</sub>	5.00 <sup>+3.37</sup> <sub>-2.18</sub>	1.30 <sup>+0.45</sup> <sub>-0.34</sub>	1.67 <sup>+1.13</sup> <sub>-0.73</sub>	2.84 <sup>+0.89</sup> <sub>-0.63</sub>	1.07	3
468	161.6623	59.2879	17.75 <sup>+3.97</sup> <sub>-3.96</sub>	12.50 <sup>+3.07</sup> <sub>-3.07</sub>	1.57 <sup>+0.49</sup> <sub>-0.35</sub>	4.81 <sup>+2.00</sup> <sub>-1.18</sub>	6.73 <sup>+1.20</sup> <sub>-1.20</sub>	0.16	1
472	161.6673	58.6292	20.50 <sup>+6.15</sup> <sub>-4.06</sub>	16.50 <sup>+4.58</sup> <sub>-4.47</sub>	1.79 <sup>+0.54</sup> <sub>-0.35</sub>	6.76 <sup>+1.88</sup> <sub>-1.83</sub>	8.46 <sup>+1.66</sup> <sub>-1.41</sub>	2.07	3
509	161.7208	59.3966	1.25 <sup>+1.12</sup> <sub>-1.02</sub>	15.50 <sup>+5.58</sup> <sub>-3.47</sub>	0.09 <sup>+0.15</sup> <sub>-0.08</sub>	11.02 <sup>+3.97</sup> <sub>-2.47</sub>	8.98 <sup>+3.31</sup> <sub>-2.26</sub>	1.22	0
523	161.7517	59.3461	3.50 <sup>+3.65</sup> <sub>-1.44</sub>	19.75 <sup>+5.79</sup> <sub>-4.19</sub>	0.26 <sup>+0.27</sup> <sub>-0.11</sub>	11.42 <sup>+3.35</sup> <sub>-2.42</sub>	5.77 <sup>+2.03</sup> <sub>-1.73</sub>	5.29	1
558	161.7836	58.6432	22.25 <sup>+5.51</sup> <sub>-4.91</sub>	32.75 <sup>+7.55</sup> <sub>-5.47</sub>	1.88 <sup>+0.46</sup> <sub>-0.41</sub>	15.53 <sup>+3.34</sup> <sub>-2.60</sub>	14.70 <sup>+2.62</sup> <sub>-1.98</sub>	2.44	3
561	161.7889	58.6454	36.25 <sup>+6.80</sup> <sub>-6.23</sub>	30.00 <sup>+6.53</sup> <sub>-5.45</sub>	3.18 <sup>+0.60</sup> <sub>-0.55</sub>	12.67 <sup>+2.76</sup> <sub>-2.30</sub>	13.93 <sup>+2.22</sup> <sub>-1.72</sub>	3.17	3
634	161.9402	59.4728	20.50 <sup>+6.15</sup> <sub>-4.06</sub>	34.75 <sup>+7.22</sup> <sub>-5.64</sub>	1.90 <sup>+0.57</sup> <sub>-0.38</sub>	18.47 <sup>+3.84</sup> <sub>-3.00</sub>	19.36 <sup>+2.91</sup> <sub>-2.71</sub>	0.83	2
636	161.9435	59.3978	2.00 <sup>+2.63</sup> <sub>-1.32</sub>	9.50 <sup>+3.60</sup> <sub>-3.46</sub>	0.16 <sup>+0.21</sup> <sub>-0.10</sub>	5.56 <sup>+2.11</sup> <sub>-2.03</sub>	4.89 <sup>+2.29</sup> <sub>-1.29</sub>	-2.00	-2
645	161.9531	59.3914	97.75 <sup>+11.18</sup> <sub>-9.44</sub>	48.75 <sup>+8.29</sup> <sub>-6.53</sub>	9.54 <sup>+1.09</sup> <sub>-0.94</sub>	19.26 <sup>+3.28</sup> <sub>-2.66</sub>	27.97 <sup>+2.63</sup> <sub>-2.32</sub>	1.56	4
712	162.0803	58.7750	6.75 <sup>+4.01</sup> <sub>-2.35</sub>	20.00 <sup>+6.53</sup> <sub>-4.44</sub>	0.52 <sup>+0.31</sup> <sub>-0.18</sub>	9.66 <sup>+2.68</sup> <sub>-2.15</sub>	10.95 <sup>+2.45</sup> <sub>-1.88</sub>	0.58	2
733	162.1368	59.2878	74.75 <sup>+9.95</sup> <sub>-8.40</sub>	44.75 <sup>+8.01</sup> <sub>-6.44</sub>	7.53 <sup>+1.00</sup> <sub>-0.85</sub>	19.25 <sup>+3.44</sup> <sub>-2.77</sub>	26.93 <sup>+2.78</sup> <sub>-2.42</sub>	1.11	1
756	162.2156	58.7401	5.00 <sup>+3.40</sup> <sub>-2.18</sub>	6.00 <sup>+3.68</sup> <sub>-2.40</sub>	1.63 <sup>+0.47</sup> <sub>-0.41</sub>	13.61 <sup>+3.39</sup> <sub>-2.55</sub>	14.46 <sup>+2.49</sup> <sub>-2.30</sub>	0.53	2
761	162.2203	58.9016	49.25 <sup>+7.79</sup> <sub>-7.23</sub>	28.50 <sup>+6.94</sup> <sub>-4.86</sub>	4.38 <sup>+0.69</sup> <sub>-0.64</sub>	10.33 <sup>+2.52</sup> <sub>-1.76</sub>	14.39 <sup>+1.81</sup> <sub>-1.70</sub>	1.13	4
762	162.2264	58.8028	9.00 <sup>+4.94</sup> <sub>-2.96</sub>	16.00 <sup>+5.08</sup> <sub>-3.97</sub>	0.74 <sup>+0.34</sup> <sub>-0.24</sub>	7.03 <sup>+2.23</sup> <sub>-1.74</sub>	4.89 <sup>+1.45</sup> <sub>-1.27</sub>	0.00	-99
763	162.2360	59.1422	12.25 <sup>+4.30</sup> <sub>-3.68</sub>	8.00 <sup>+3.94</sup> <sub>-2.78</sub>	1.53 <sup>+0.54</sup> <sub>-0.46</sub>	4.45 <sup>+2.19</sup> <sub>-1.55</sub>	5.73 <sup>+1.74</sup> <sub>-1.25</sub>	-1.00	-1
764	162.2364	58.8562	12.75 <sup>+4.94</sup> <sub>-3.32</sub>	15.50 <sup>+5.58</sup> <sub>-3.47</sub>	0.34 <sup>+0.23</sup> <sub>-0.18</sub>	2.42 <sup>+1.61</sup> <sub>-0.90</sub>	2.16 <sup>+1.06</sup> <sub>-0.75</sub>	0.00	-99
765	162.2370	58.8560	16.00 <sup>+5.08</sup> <sub>-3.97</sub>	20.00 <sup>+5.54</sup> <sub>-4.44</sub>	1.27 <sup>+0.40</sup> <sub>-0.32</sub>	7.83 <sup>+2.17</sup> <sub>-1.74</sub>	7.66 <sup>+1.79</sup> <sub>-1.27</sub>	0.00	-99
766	162.2384	58.9408	4.50 <sup>+3.87</sup> <sub>-1.88</sub>	2.50 <sup>+3.41</sup> <sub>-1.16</sub>	0.47 <sup>+0.28</sup> <sub>-0.19</sub>	5.04 <sup>+2.02</sup> <sub>-1.50</sub>	3.28 <sup>+1.42</sup> <sub>-0.92</sub>	0.00	-99
767	162.2402	58.8784	8.75 <sup>+4.35</sup> <sub>-2.71</sub>	5.75 <sup>+3.83</sup> <sub>-2.15</sub>	0.72 <sup>+0.36</sup> <sub>-0.22</sub>	2.02 <sup>+1.34</sup> <sub>-0.75</sub>	2.28 <sup>+0.87</sup> <sub>-0.65</sub>	0.00	-99
768	162.2450	58.9788	94.25 <sup>+10.48</sup> <sub>-9.33</sub>	32.50 <sup>+7.30</sup> <sub>-5.22</sub>	9.89 <sup>+1.10</sup> <sub>-0.94</sub>	12.05 <sup>+2.71</sup> <sub>-1.98</sub>	22.29 <sup>+2.16</sup> <sub>-1.98</sub>	1.36	3
769	162.2452	59.1244	50.25 <sup>+7.87</sup> <sub>-7.30</sub>	26.00 <sup>+6.16</sup> <sub>-5.07</sub>	4.66 <sup>+0.73</sup> <sub>-0.68</sub>	9.32 <sup>+2.21</sup> <sub>-1.82</sub>	14.04 <sup>+1.81</sup> <sub>-1.62</sub>	-1.00	-1
770	162.2460	58.8365	24.75 <sup>+6.31</sup> <sub>-4.72</sub>	23.25 <sup>+5.61</sup> <sub>-5.02</sub>	2.03 <sup>+0.52</sup> <sub>-0.39</sub>	8.66 <sup>+2.09</sup> <sub>-1.87</sub>	11.06 <sup>+1.92</sup> <sub>-1.46</sub>	0.00	-99
771	162.2533	59.0769	15.25 <sup>+4.70</sup> <sub>-4.09</sub>	0.00 <sup>+21.95</sup> <sub>-0.00</sub>	1.37 <sup>+0.42</sup> <sub>-0.37</sub>	0.00 <sup>+0.00</sup> <sub>-10.32</sub>	4.73 <sup>+1.46</sup> <sub>-1.27</sub>	-1.00	-1
772	162.2644	59.0021	15.00 <sup>+4.95</sup> <sub>-3.84</sub>	6.00 <sup>+3.58</sup> <sub>-2.40</sub>	0.63 <sup>+0.34</sup> <sub>-0.21</sub>	3.31 <sup>+1.48</sup> <sub>-1.22</sub>	2.90 <sup>+1.18</sup> <sub>-0.78</sub>	-1.00	-1
773	162.2718	58.8679	22.00 <sup>+3.94</sup> <sub>-4.66</sub>	7.50 <sup>+4.44</sup> <sub>-2.28</sub>	2.62 <sup>+0.69</sup> <sub>-0.56</sub>	2.79 <sup>+1.65</sup> <sub>-0.85</sub>	4.91 <sup>+1.22</sup> <sub>-0.85</sub>	3.44	4
774	162.2795	58.9679	0.50 <sup>+2.79</sup> <sub>-0.37</sub>	4.75 <sup>+3.62</sup> <sub>-1.93</sub>	0.04 <sup>+0.22</sup> <sub>-0.03</sub>	3.22 <sup>+2.46</sup> <sub>-1.31</sub>	1.36 <sup>+1.43</sup> <sub>-0.95</sub>	0.75	3
775	162.2949	58.8574	9.75 <sup>+4.61</sup> <sub>-2.87</sub>	8.50 <sup>+4.60</sup> <sub>-2.46</sub>	0.83 <sup>+0.38</sup> <sub>-0.24</sub>	3.22 <sup>+1.75</sup> <sub>-0.93</sub>	3.96 <sup>+1.24</sup> <sub>-0.88</sub>	0.99	1
776	162.2998	59.0320	51.25 <sup>+7.94</sup> <sub>-7.37</sub>	17.50 <sup>+5.82</sup> <sub>-3.71</sub>	5.54 <sup>+0.86</sup> <sub>-0.80</sub>	6.63 <sup>+2.20</sup> <sub>-1.41</sub>	12.19 <sup>+1.63</sup> <sub>-1.53</sub>	-1.00	-1
777	162.3024	58.8895	18.00 <sup>+5.32</sup> <sub>-4.21</sub>	6.50 <sup>+4.26</sup> <sub>-2.10</sub>	1.68 <sup>+0.50</sup> <sub>-0.39</sub>	2.14 <sup>+1.41</sup> <sub>-0.69</sub>	3.83 <sup>+0.90</sup> <sub>-0.81</sub>	0.00	-99
778	162.3048	58.9967	17.25 <sup>+4.95</sup> <sub>-4.34</sub>	25.75 <sup>+6.41</sup> <sub>-4.82</sub>	0.54 <sup>+0.35</sup> <sub>-0.17</sub>	5.76 <sup>+2.02</sup> <sub>-1.73</sub>	5.51 <sup>+1.58</sup> <sub>-1.39</sub>	-1.00	-1
779	162.3198	58.8593	7.25 <sup>+3.51</sup> <sub>-2.85</sub>	13.00 <sup>+4.69</sup> <sub>-3.57</sub>	0.03 <sup>+0.19</sup> <sub>-0.02</sub>	15.50 <sup>+4.97</sup> <sub>-3.21</sub>	17.38 <sup>+4.80</sup> <sub>-3.53</sub>	0.00	-99
780	162.3240	58.8417	11.25 <sup>+4.16</sup> <sub>-3.53</sub>	21.25 <sup>+5.40</sup> <sub>-4.81</sub>	0.97 <sup>+0.36</sup> <sub>-0.30</sub>	10.14 <sup>+2.58</sup> <sub>-2.29</sub>	9.87 <sup>+2.05</sup> <sub>-1.86</sub>	0.00	-99
781	162.3285	58.8992	37.25 <sup>+6.88</sup> <sub>-6.31</sub>	12.75 <sup>+4.94</sup> <sub>-3.32</sub>	3.89 <sup>+0.72</sup> <sub>-0.66</sub>	4.66 <sup>+1.81</sup> <sub>-1.21</sub>	8.61 <sup>+1.45</sup> <sub>-1.18</sub>	0.21	1
782	162.3314	58.9806	43.75 <sup>+9.33</sup> <sub>-6.36</sub>	27.50 <sup>+5.76</sup> <sub>-5.67</sub>	4.57 <sup>+0.83</sup> <sub>-0.67</sub>	12.53 <sup>+2.62</sup> <sub>-2.59</sub>	17.20 <sup>+3.39</sup> <sub>-1.90</sub>	1.79	4
783	162.3320	58.7839	114.25 <sup>+11.46</sup> <sub>-10.92</sub>	48.00 <sup>+7.97</sup> <sub>-6.91</sub>	10.97 <sup>+1.10</sup> <sub>-1.05</sub>	16.98 <sup>+2.82</sup> <sub>-2.44</sub>	27.42 <sup>+2.36</sup> <sub>-2.18</sub>	2.36	3
784	162.3330	58.7929	6.50 <sup>+4.26</sup> <sub>-2.10</sub>	12.25 <sup>+4.30</sup> <sub>-3.68</sub>	1.45 <sup>+0.58</sup> <sub>-0.43</sub>	0.20 <sup>+0.68</sup> <sub>-0.16</sub>	1.40 <sup>+0.47</sup> <sub>-0.40</sub>	0.00	-99
785	162.3517	58.7906	11.00 <sup>+4.41</sup> <sub>-3.28</sub>	0.75 <sup>+2.54</sup> <sub>-0.62</sub>	1.51 <sup>+0.49</sup> <sub>-0.35</sub>	5.39 <sup>+1.81</sup> <sub>-1.55</sub>	6.83 <sup>+1.38</sup> <sub>-1.36</sub>	0.00	-99
786	162.3532	58.8503	8.50 <sup>+4.60</sup> <sub>-2.46</sub>	4.00 <sup>+3.15</sup> <sub>-1.94</sub>	0.42 <sup>+0.16</sup> <sub>-0.16</sub>	0.95 <sup>+0.36</sup> <sub>-0.44</sub>	0.90 <sup>+0.77</sup> <sub>-0.33</sub>	0.00	-99
787	162.3717	58.8940	838.75 <sup>+30.23</sup> <sub>-28.71</sub>	239.75 <sup>+16.76</sup> <sub>-15.23</sub>	90.78 <sup>+3.27</sup> <sub>-3.11</sub>	86.92 <sup>+6.08</sup> <sub>-5.52</sub>	176.46 <sup>+5.64</sup> <sub>-5.38</sub>	0.25	4
788	162.3815	58.8004	16.75 <sup>+5.45</sup> <sub>-4.84</sub>	13.25 <sup>+4.44</sup> <sub>-3.82</sub>	1.48 <sup>+0.52</sup> <sub>-0.44</sub>	2.99 <sup>+1.59</sup> <sub>-1.27</sub>	4.44 <sup>+1.42</sup> <sub>-0.92</sub>	-1.00	-1
789	162.4150	58.8908	12.25 <sup>+4.30</sup> <sub>-3.68</sub>	6.25 <sup>+3.33</sup> <sub>-2.65</sub>	2.03 <sup>+0.56</sup> <sub>-0.41</sub>	6.40 <sup>+2.30</sup> <sub>-1.43</sub>	6.67 <sup>+1.41</sup> <sub>-1.28</sub>	-1.00	-1

NOTE. —

<sup>a</sup>Units of  $10^{-15} \text{ erg cm}^{-2} \text{ s}^{-1}$ .

$z_{spec} = 0$  and corresponding class = -99, source spectroscopically observed but neither the redshift nor the class could be identified.

$z_{spec} = -1$  and corresponding class = -1, source not yet spectroscopically observed.

$z_{spec} = -2$  and corresponding class = -2, source is a star.

class = 0, absorbers; class = 1, star formers; class = 3, high-excitation sources; class = 4, BLAGNs.

TABLE 3  
OPTICAL SPECTRAL CLASSIFICATION FOR OUR 2 – 8 keV SAMPLE  
BY FIELD AND OPTICAL SPECTRAL TYPE

Category	CLANS (407)	CLASXS (251)	CDF-N (87)	All (745)
Observed	331	235	85	651
Identified	243	162	64	469
Unidentified	88	73	21	182
Unidentified with phot-zs	51	43	18	112
BLAGN <sup>a</sup>	106 (43%)	77 (47%)	24 (38%)	207 (44%)
HEX <sup>a</sup>	72 (30%)	35 (22%)	11 (17%)	118 (25%)
SF <sup>a</sup>	51 (21%)	34 (21%)	19 (30%)	104 (22%)
ABS <sup>a</sup>	13 (5%)	12 (7%)	8 (13%)	33 (7%)
Star	1	4	1	6

<sup>a</sup>The percentages refer to the percent of identified sources that exhibit the specified spectral type.

Alexander et al. 2002; Bauer et al. 2002; Barger et al. 2003). As expected, the majority of our spectroscopically observed but unidentified sources (black circles) have faint optical magnitudes ( $> 70\%$  have  $R > 24$ ). In obtaining our spectroscopy, we selected the sources without any regard to their optical magnitudes in order to avoid additional selection effects. This is evident from the figure, where the spectroscopically unobserved sources (yellow circles) cover the entire range of optical magnitudes. We will not show these sources in our subsequent figures nor use them in our subsequent analysis, as they can be considered a random sample of the population and will not affect our results. Thus, in Figure 3 we show the fraction of spectroscopically observed sources in our 2 – 8 keV sample that are spectroscopically identified versus X-ray flux.

In Trouille et al. (2008) we extended the redshift information for the three fields by determining photometric redshifts. The CLANS field has eight bands of coverage ( $g', r', i', z', J, H, K, 3.6 \mu\text{m}$ ), the CLASXS field has 11 bands of coverage ( $u, B, g', V, R, i', z', J, H, K, 3.6 \mu\text{m}$ ), and the CDF-N field has 10 bands of coverage ( $U, B, V, R, I, z', J, H, K_s, 3.6 \mu\text{m}$ ). We used the template-fitting method described in Wang et al. (2006, and references therein). We built our training set of spectral energy distributions (SEDs) using the spectroscopically identified sources in our sample. We then determined the photometric redshifts by finding the best fit (via least-squares minimization) between our individual source SEDs (using the optical through infrared data) and these templates. We include the number of photometric redshifts for the spectroscopically observed but unidentified sources obtained in this way as an entry in Table 3.

In Figure 4 we show the redshift distributions for our spectroscopically observed 2 – 8 keV sample by optical spectral type (all, BLAGN, non-BLAGN). The shaded areas show the spectroscopically identified distributions, while the solid line in (a) shows the spectroscopically plus photometrically identified distribution. The non-BLAGN redshift distribution is strongly peaked at  $z \sim 0.9$ .

#### 4. COMPARISON OF OPTICAL CLASSIFICATION WITH X-RAY CLASSIFICATION

##### 4.1. $\Gamma_{\text{eff}}$ Distributions

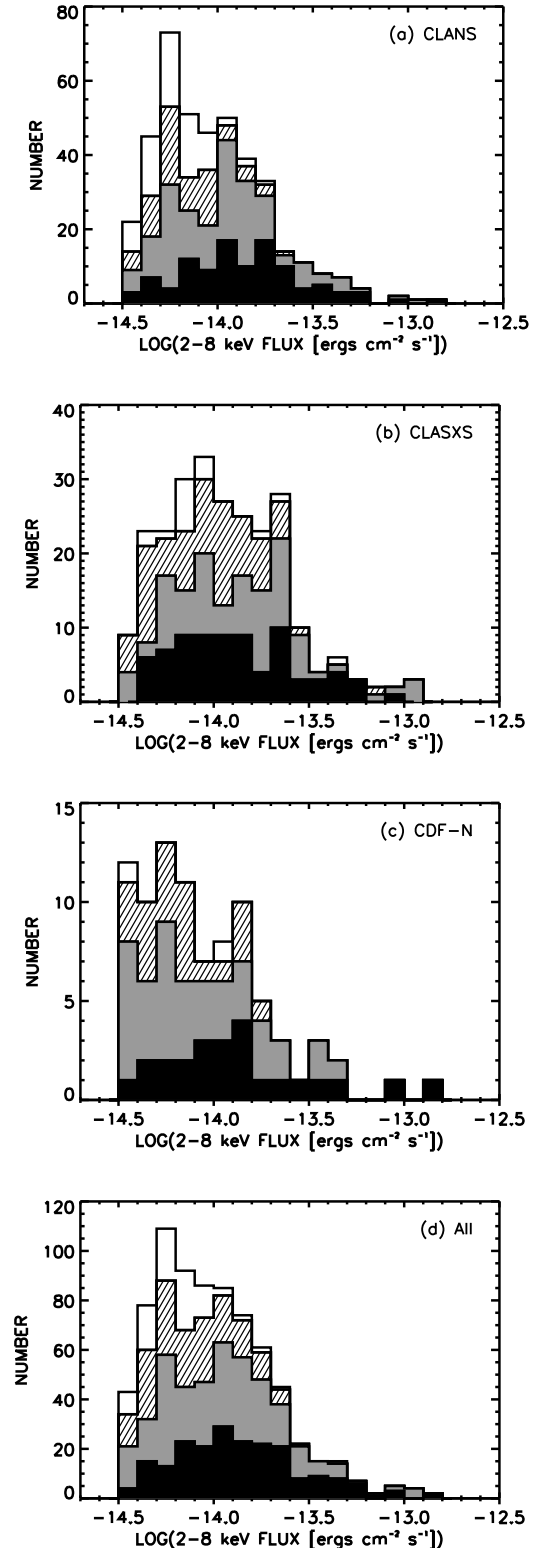


FIG. 1.— 2 – 8 keV flux distributions for our (a) CLANS, (b) CLASXS, (c) CDF-N, and (d) total 2 – 8 keV sample (black, spectroscopically identified BLAGNs; shaded, spectroscopically identified non-BLAGNs; hatched, spectroscopically observed but unidentified sources; open, spectroscopically unobserved sources).

In Figure 5 we show the  $\Gamma_{\text{eff}}$  distributions for the spectroscopically observed sources in our 2 – 8 keV sample by

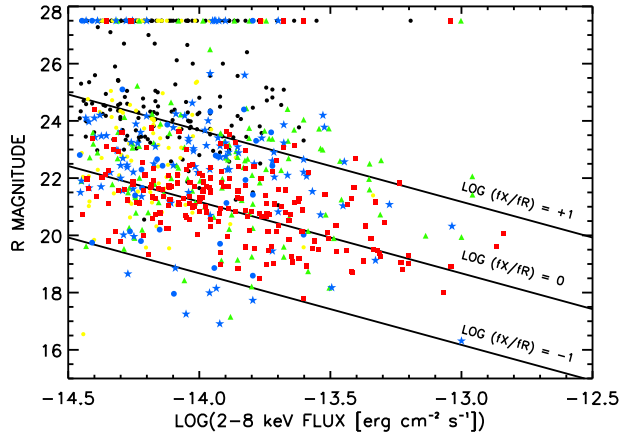


FIG. 2.—  $R$  magnitude vs. 2–8 keV flux for our 2–8 keV sample (red squares, BLAGNs; green triangles, high-excitation sources; blue circles, absorbers; blue stars, star formers; black circles, spectroscopically observed but unidentified sources; yellow circles, spectroscopically unobserved sources). Solid lines show where the fluxes are equal [i.e.,  $\log(f_X)/f_R = 0$ ] and the boundaries of the region where AGNs typically reside [ $\log(f_X)/f_R = \pm 1$ ]. Magnitudes brighter than  $R \sim 20$  suffer from saturation problems and are likely to be underestimated. Sources undetected at the  $2\sigma$  limits of the images are plotted at  $R = 27.5$ .

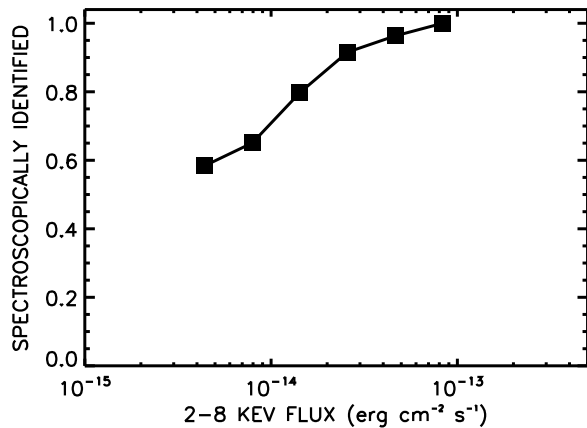


FIG. 3.— Fraction of spectroscopically observed sources in our 2–8 keV sample that are spectroscopically identified in bins of 2–8 keV flux. Only bins which contain five or more sources are plotted. Due to the complicated observing program for the CDF-N, all sources in that field are treated as spectroscopically observed, though we note that there are only two sources that have not been observed (see Figure 1).

optical spectral type (BLAGN, HEX, ABS+SF, unidentified). For the CLANS sources we used the  $\Gamma_{\text{eff}}$  values given in Trouille et al. (2008), and for the CDF-N sources we used the  $\Gamma_{\text{eff}}$  values given in Alexander et al. (2003). To determine the  $\Gamma_{\text{eff}}$  values for the CLASXS sources we followed the method used by Trouille et al. (2008). In short, from the HRs given in Yang et al. (2004) and using XSPEC, we determined the HR-to- $\Gamma_{\text{eff}}$  conversion by assuming a single power law spectrum with Galactic absorption.

We see from Figure 5 that there is substantial overlap in the  $\Gamma_{\text{eff}}$  distributions for the BLAGNs and the non-BLAGNs. We also note that the spectroscopically

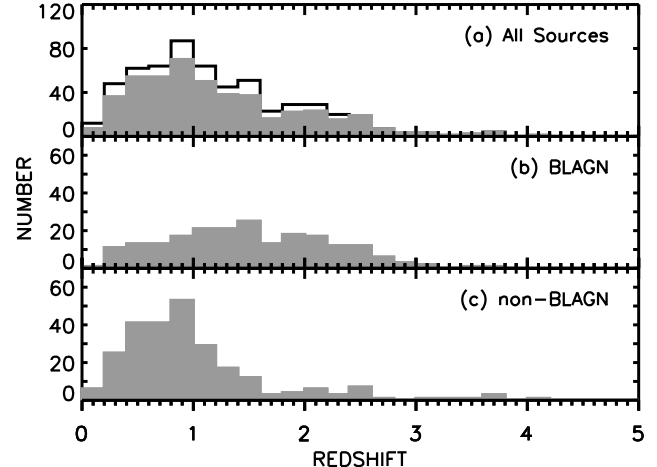


FIG. 4.— Redshift distributions for our spectroscopically observed 2–8 keV sample by optical spectral type. The shaded area shows (a) all spectroscopic redshifts, (b) BLAGNs, and (c) non-BLAGNs. The solid line in (a) shows the spectroscopic plus photometric redshift distribution.

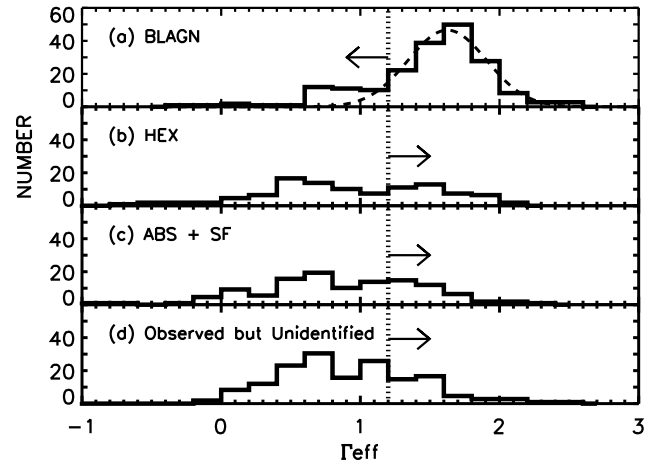


FIG. 5.—  $\Gamma_{\text{eff}}$  distributions for the BLAGNs, the high-excitation sources, the absorbers plus star formers, and the unidentified sources in our spectroscopically observed 2–8 keV sample. The dashed curve shows the gaussian fit to the  $\Gamma_{\text{eff}}$  distribution for the BLAGNs ( $\langle \Gamma_{\text{eff}} \rangle = 1.63$  and  $\sigma = 0.28$ ). The vertical dotted line shows  $\Gamma_{\text{eff}} = 1.2$ . The arrows indicate the locations of the outlier sources discussed in Section 4.

unidentified sources have a  $\Gamma_{\text{eff}}$  distribution which is very similar to the HEX and ABS+SF sources.

The dashed curve in Figure 5(a) shows the gaussian fit to the  $\Gamma_{\text{eff}}$  distribution for the BLAGNs. We find that the BLAGNs are clustered around  $\langle \Gamma_{\text{eff}} \rangle = 1.63$  with a dispersion  $\sigma = 0.28$ . Mushotzky (1984) was the first to note this narrow range in photon indices. The vertical line at  $\Gamma_{\text{eff}} = 1.2$  indicates the value above which 80% of the BLAGNs reside. As noted in the Introduction,  $\Gamma_{\text{eff}} = 1.2$  is approximately equivalent to  $\text{HR} = -0.2$ , which is the value Szokoly et al. (2004) chose to use to distinguish between X-ray type 1 (unabsorbed) sources and X-ray type 2 (absorbed) sources.

#### 4.1.1. Optically Unobscured but X-ray Absorbed

As is well known (see references in the Introduction), despite the generally good agreement between the two classification schemes regarding which sources are

unabsorbed, the agreement is not 100%. There are BLAGNs whose X-ray spectral properties suggest substantial absorption. In our spectroscopically observed 2 – 8 keV sample, we find that  $20\% \pm 3\%$  of the 207 BLAGNs have  $\Gamma_{\text{eff}} < 1.2$ . The leftward pointing arrow in Figure 5(a) calls attention to these BLAGNs with low values of  $\Gamma_{\text{eff}}$ , all of which have at least one emission line with  $\text{FWHM} > 2000 \text{ km s}^{-1}$ . The optical spectra of these sources do not appear to share any common characteristics, nor do they appear any different than the spectra for our BLAGNs with  $\Gamma_{\text{eff}} \geq 1.2$ . Only one of these sources (CLASXS #174) has less than 10 counts at 0.5 – 8 keV and may suffer from contamination by uncleared afterglow events (see <http://asc.harvard.edu/ciao/why/afterglow.html>).

Kuraszkiewicz et al. (2009a,b) studied a sample of red AGNs that they selected from the Two Micron All Sky Survey (2MASS) on the basis of their red  $J-K_s$  colors ( $> 2$  mag) and then followed up with *Chandra*. 85% of their  $J-K > 2$  sample show broad-lines, and the remainder are narrow-line AGNs. Through detailed modeling they found that the shape of the SEDs for these sources was generally consistent with modest absorption by gas (in X-rays) and dust (in the optical/NIR). Using principal component analysis, they argue that the Eddington ratio (and not absorption by the circumnuclear material or the host galaxy) is the dominant factor in determining the shape of the SED.

We can use our color information to look for color differences between our X-ray absorbed and X-ray unabsorbed BLAGNs to test for extinction associated with low  $\Gamma_{\text{eff}}$  values (assuming the low  $\Gamma_{\text{eff}}$  value is due to absorption by gas along the line-of-sight). In Figure 6 we show  $I-J$  versus  $J-K$  for the BLAGNs in our spectroscopically observed 2 – 8 keV sample. To avoid  $K$ -correction effects in the comparison, we divide our sample by redshift. In each redshift interval we see no significant differences in the color distributions of the  $\Gamma_{\text{eff}} < 1.2$  and  $\Gamma_{\text{eff}} \geq 1.2$  BLAGNs. This provides support for the suggestion that there is not a one-to-one correspondence between  $\Gamma_{\text{eff}}$  and extinction (Cowie et al. 2009; see also Maiolino et al. 2001 and Kuraszkiewicz et al. 2009b).

#### 4.1.2. Optically Obscured but X-ray Unabsorbed

As is also well known (see references in the Introduction), there are a number of sources whose optical spectra do not show broad lines, suggesting obscuration, while their X-ray spectral properties suggest little absorption. In our spectroscopically observed 2 – 8 keV sample,  $33\% \pm 4\%$  of the 255 non-BLAGNs have  $\Gamma_{\text{eff}} \geq 1.2$ . The rightward pointing arrows in Figures 5(b), (c), and (d) call attention to these non-BLAGNs with high values of  $\Gamma_{\text{eff}}$ . The optical spectra for these sources do not appear any different than the spectra for our non-BLAGNs with  $\Gamma_{\text{eff}} < 1.2$ . All of these sources have more than 10 counts at 0.5 – 8 keV.

We may look at the most extreme examples of conflicting optical and X-ray information by considering the 22 non-BLAGNs with  $\Gamma_{\text{eff}} \geq 1.7$ . Considering in detail the optical spectra of the individual non-BLAGNs in our 2 – 8 keV sample having  $\Gamma_{\text{eff}} \geq 1.7$ , we find that all have spectra covering at least one of the poten-

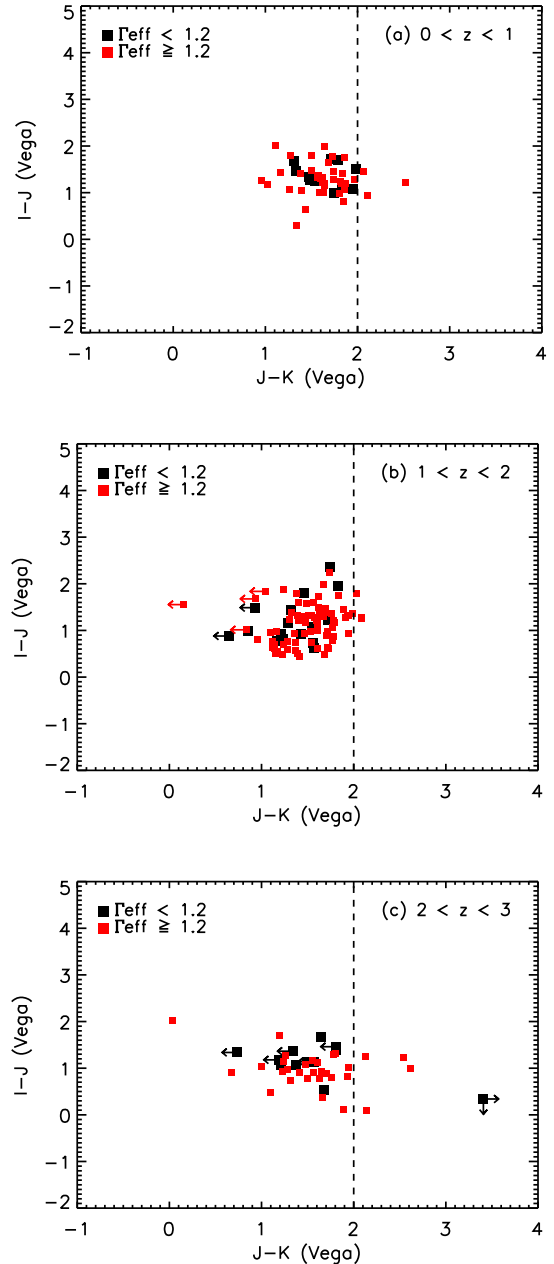


FIG. 6.—  $I-J$  vs.  $J-K$  for the BLAGNs in our spectroscopically observed 2 – 8 keV sample in the redshift intervals (a)  $0 < z < 1$ , (b)  $1 < z < 2$ , and (c)  $2 < z < 3$ . BLAGNs with  $\Gamma \geq 1.2$  are shown in red, while BLAGNs with  $\Gamma < 1.2$  are shown in black. Sources undetected in two or more of the three bands are not shown. Sources with leftward pointing arrows were not detected above the limiting magnitude in the  $K$  band of their respective field. The source in (c) with a rightward pointing arrow and a downward pointing arrow was not detected above the limiting magnitude in the  $J$  band of the CLANS field (CLANS #301).

tially broadened emission lines (i.e.,  $\text{H}\alpha$ ,  $\text{H}\beta$ ,  $\text{H}\gamma$ ,  $\text{MgII}$ ,  $\text{Ly}\alpha$ , and  $\text{CIV}$ ). All but two of the HEX sources exhibit  $\text{FWHM} < 1500 \text{ km s}^{-1}$  (CDF-N #301 and CDF-N #331 exhibit  $1500 < \text{FWHM} < 1900 \text{ km s}^{-1}$ ). Moreover, all of the optically spectroscopically identified absorbers can be confidently classified as non-BLAGNs, as can all but one of the star formers (CLANS #71 lacks sufficient signal-to-noise at the wavelengths of the potentially



broadened emission lines covered by its spectrum).

#### 4.2. $\Gamma_{\text{eff}}$ versus X-ray Luminosity

In Section 4.1 we found that while  $80\% \pm 6\%$  of the BLAGNs in our sample have  $\Gamma_{\text{eff}} \geq 1.2$ ,  $33\% \pm 4\%$  of our non-BLAGNs also have  $\Gamma_{\text{eff}} \geq 1.2$ . We now expand our spectroscopically observed 2–8 keV sample to include *ASCA* large-area, bright-flux data (hereafter, we refer to this larger sample as our “extended spectroscopically observed 2–8 keV sample”). These additional data are needed to have a sufficiently large volume at the high-luminosity, low-redshift end.

We use the optical spectral classifications, redshifts, X-ray luminosities, and  $\Gamma_{\text{eff}}$  values from Akiyama et al. (2003; 75 optically identified AMSSn AGNs) and Akiyama et al. (2000; 30 optically identified ALSS AGNs). We converted their 2–10 keV luminosities into rest-frame 2–8 keV luminosities using

$$L_{2-8 \text{ keV}} = \frac{\int_{2 \text{ keV}}^{8 \text{ keV}} \nu^{-\Gamma_{\text{eff}}} d\nu}{\int_{2 \text{ keV}}^{10 \text{ keV}} \nu^{-\Gamma_{\text{eff}}} d\nu} \times L_{2-10 \text{ keV}} \quad (1)$$

and the  $\Gamma_{\text{eff}}$  for each source.  $L_{2-8 \text{ keV}}$  is on average  $\approx 90\%$  of  $L_{2-10 \text{ keV}}$ . We calculated the rest-frame 2–8 keV luminosities for our three OPTX fields using  $L_X = f \times 4\pi d_L^2 \times K$ -correction. Assuming an intrinsic  $\Gamma = 1.8$ , we used

for  $z < 3$ ,  $K\text{-corr} = (1+z)^{-0.2}$  and  $f = f_{2-8 \text{ keV}}$ ,

for  $z \geq 3$ ,  $K\text{-corr} = \left[ \frac{1}{4}(1+z) \right]^{-0.2}$  and  $f = f_{0.5-2 \text{ keV}}$ .

The  $\frac{1}{4}$  factor in the  $z \geq 3$   $K$ -correction is a result of normalizing so that there is no  $K$ -correction when  $z = 3$ , at which point observed-frame 0.5–2 keV corresponds exactly to rest-frame 2–8 keV.

In Figure 7 (upper panel) we plot  $\Gamma_{\text{eff}}$  versus rest-frame 2–8 keV luminosity for our extended spectroscopically observed 2–8 keV sample, and in Figure 7 (lower panel) we plot  $\langle \Gamma_{\text{eff}} \rangle$  versus rest-frame 2–8 keV luminosity. According to Hasinger et al. (2005)’s mixed classification scheme described in the Introduction, any source above the dashed horizontal line ( $\Gamma_{\text{eff}} = 1.2$ ) would be considered unabsorbed, and any source below (other than optically classified BLAGNs) would be considered absorbed. (Of course, to be able to exclude the BLAGNs that lie below the line from the absorbed category—or to be able to include them in the unabsorbed category—requires high optical spectroscopic completeness.) We can see that their method picks up most of its ‘new’ (above the line) unabsorbed sources (as compared with what would be found from a pure optical classification scheme) at lower X-ray luminosities. However, it also picks up a large number of HEX sources at higher X-ray luminosities. Since we do not yet have a good understanding of how the X-ray and optical classification schemes relate to the obscuration of the central engine, mixing the two classification schemes in this manner can only complicate the interpretation, and we strongly advise against it.

From Figure 7 (upper panel) we see the well-known luminosity dependence of the optical spectral types, with the BLAGNs dominating the numbers at high X-ray luminosities (Lawrence & Elvis 1982; Steffen et al. 2003;

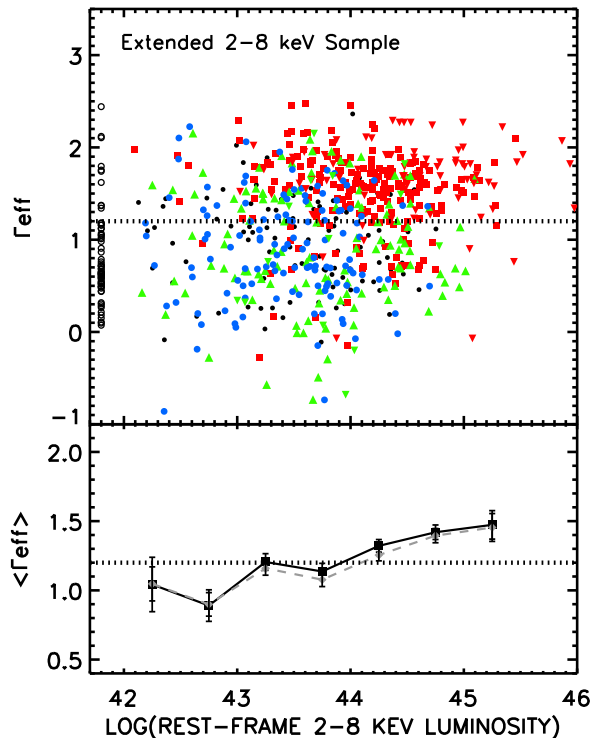


FIG. 7.— (Upper panel)  $\Gamma_{\text{eff}}$  vs. rest-frame 2–8 keV luminosity for the sources in our extended spectroscopically observed 2–8 keV sample (red squares, BLAGNs; red inverted triangles, *ASCA* BLAGNs; green triangles, high-excitation sources; green inverted triangles, *ASCA* non-BLAGNs; blue circles, absorbers and star-formers; black solid circles, spectroscopically observed but unidentified sources with photometric redshifts; black open circles plotted at a nominal luminosity, spectroscopically observed but unidentified sources without photometric redshifts). (Lower panel)  $\langle \Gamma_{\text{eff}} \rangle$  in luminosity bins vs. rest-frame 2–8 keV luminosity. The spectroscopic sample is denoted by the black symbols and solid lines, while the spectroscopic plus photometric sample is denoted by the gray symbols and dashed lines. Only bins with at least six sources are plotted. The error bars show  $\frac{1}{\sqrt{N}}$ . The dotted horizontal lines in both panels show  $\Gamma_{\text{eff}} = 1.2$ .

Ueda et al. 2003; Barger et al. 2005; La Franca et al. 2005; Simpson 2005; Akylas et al. 2006; Beckmann et al. 2006; Sazonov et al. 2007; Della Ceca et al. 2008; Hasinger 2008; Silverman et al. 2008; Winter et al. 2009; Yencho et al. 2009). From Figure 7 (lower panel) we see there is also a luminosity dependence of the effective X-ray photon index, with  $\langle \Gamma_{\text{eff}} \rangle$  rising from  $\sim 1$  at  $L_X = 10^{42} \text{ erg s}^{-1}$  to  $\sim 1.5$  at  $L_X = 10^{45} \text{ erg s}^{-1}$ .

In Figure 8 we divide Figure 7 into three redshift intervals: (a)  $z = 0.1 - 0.5$ , (b)  $z = 0.5 - 1$ , and (c)  $z = 1 - 3$ . Although the distributions in the upper panels of the figure look the same for each redshift interval, we can see that the transition luminosity from X-ray soft ( $\Gamma_{\text{eff}} \geq 1.2$ ) dominated to X-ray hard dominated (or from BLAGN dominated to non-BLAGN dominated) is shifting to higher luminosities with increasing redshift interval. This redshift dependence of the transition luminosity was first noted by Barger et al. (2005; see their Figure 19) from the luminosity functions.

In the lower panels of Figure 8 we see that for the two lower redshift intervals there is a dominance of the X-ray



TABLE 4  
NON-BLAGNS WITH SOFT PHOTON INDICES IN OUR EXTENDED SPECTROSCOPICALLY OBSERVED 2 – 8 KEV SAMPLE BY REDSHIFT INTERVAL

$\Gamma_{\text{eff}}$	HEX <sup>a</sup>	SF <sup>a</sup>	ABS <sup>a</sup>
$z < 1$			
All	74	60	30
$\geq 1.2$	27 (36%)	16 (26%)	7 (23%)
$\geq 1.5$	15 (20%)	6 (10%)	4 (13%)
$\geq 1.7$	7 (10%)	3 (5%)	2 (7%)
$1 < z < 3$			
All	37	41	3
$\geq 1.2$	15 (41%)	18 (44%)	0 (0%)
$\geq 1.5$	9 (24%)	8 (20%)	0 (0%)
$\geq 1.7$	7 (19%)	3 (7%)	0 (0%)

<sup>a</sup>The percentages refer to the percent of sources of the given optical spectral type with the specified values for  $\Gamma_{\text{eff}}$ .

soft sources at higher luminosities and a decreasing influence of these sources at lower luminosities, as previously noted from Figure 7. However, in the  $z = 1 - 3$  interval we instead see a continued dominance of the soft sources at lower luminosities. This is in part due to the fact that at higher redshifts the 2 – 8 keV band samples higher energies, and these higher energies are less affected by obscuring material (see Kim et al. 2007 for modeling of this effect). Thus, a higher percentage of  $z > 1$  non-BLAGNs are X-ray soft (have high  $\Gamma_{\text{eff}}$ ) compared with those at  $z < 1$ , as Szokoly et al. (2004) cautioned when they were defining their X-ray classification scheme (see Introduction). This emphasizes the danger in using the highly redshift-dependent hardness ratio for classifying sources as absorbed or unabsorbed, as is done in both the pure X-ray classification and mixed classification schemes.

In Table 4 we give the percentages of high-excitation sources, star formers, and absorbers with  $z < 1$  and  $1 < z < 3$  in our extended spectroscopically observed 2 – 8 keV sample with  $\Gamma_{\text{eff}} \geq 1.2$ ,  $\Gamma_{\text{eff}} \geq 1.5$ , and  $\Gamma_{\text{eff}} \geq 1.7$ . The non-BLAGNs in the  $1 < z < 3$  redshift interval exhibit a higher percentage of X-ray soft sources than the  $z < 1$  redshift interval (the exception being the absorbers, which suffer from small numbers in the  $z = 1 - 3$  interval).

## 5. DISCUSSION

Using our large spectroscopically observed 2 – 8 keV sample with  $> 80\%$  spectroscopic completeness for  $f_{2-8 \text{ keV}} > 10^{-14} \text{ erg cm}^{-2} \text{ s}^{-1}$  and  $> 60\%$  spectroscopic completeness down to our chosen flux limit of  $f_{2-8 \text{ keV}} = 3.5 \times 10^{-15} \text{ erg cm}^{-2} \text{ s}^{-1}$ , we have confirmed that there is considerable overlap of the X-ray spectral properties for different optical spectral types. For example, although  $80\% \pm 6\%$  of the BLAGNs in our sample have  $\Gamma_{\text{eff}} \geq 1.2$ , so do  $36\% \pm 6\%$  of our HEX sources and  $30\% \pm 5\%$  of our absorbers and star formers. (Of course, this also means that  $20\% \pm 3\%$  of the BLAGNs in our sample have  $\Gamma_{\text{eff}} < 1.2$ .) Even considering a more extreme X-ray softness cut-off, we still find that  $12\% \pm 3\%$  of the HEX sources and  $6\% \pm 2\%$  of the absorbers and star formers in our sample have  $\Gamma_{\text{eff}} \geq 1.7$ . A number of authors have suggested possible ways to account for this overlap through observational problems. In this section we briefly consider these and conclude that they are not major contributors to the overlap.

X-ray spectral variability has been suggested as a pos-

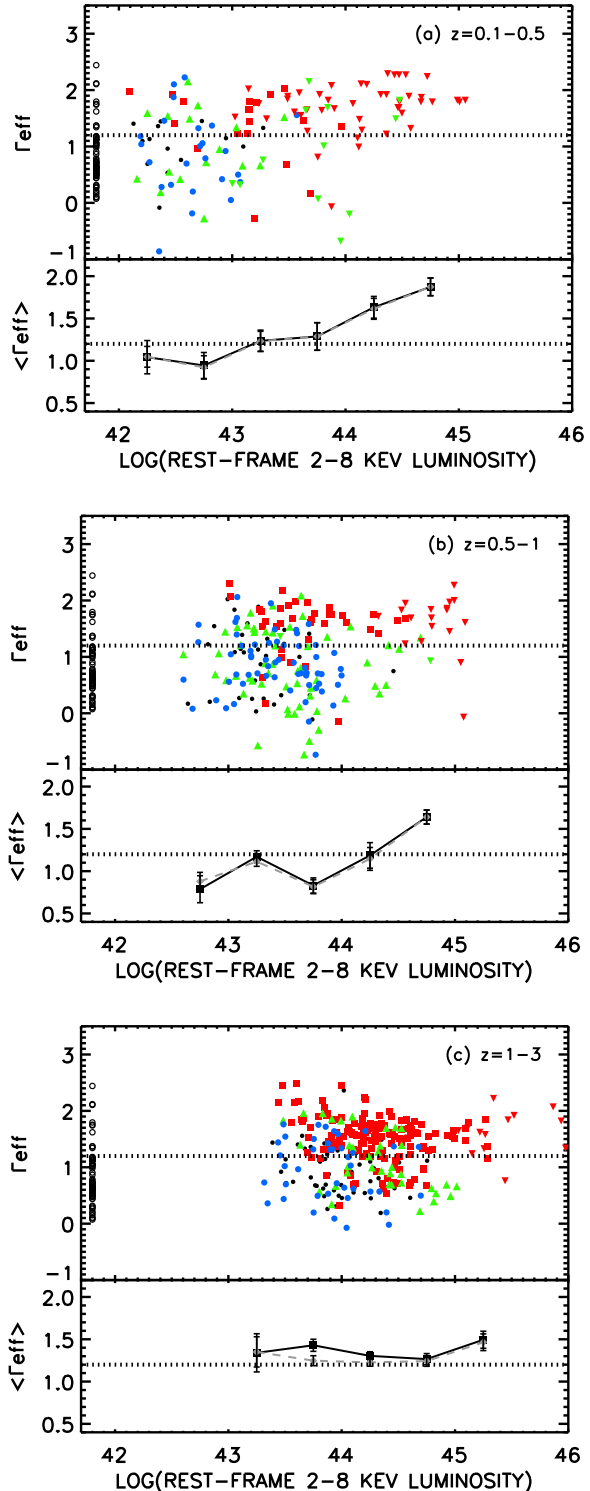


FIG. 8.— (Upper panels)  $\Gamma_{\text{eff}}$  vs. rest-frame 2 – 8 keV luminosity for the sources in our extended spectroscopically observed 2 – 8 keV sample with (a)  $z = 0.1 - 0.5$ , (b)  $z = 0.5 - 1$ , and (c)  $z = 1 - 3$ . (Lower panels)  $\langle \Gamma_{\text{eff}} \rangle$  in luminosity bins vs. rest-frame 2 – 8 keV luminosity. Only bins with at least six sources are plotted. The error bars show  $\frac{1}{\sqrt{N}}$ . In both sets of panels the symbols are the same as in Figure 7.

sible explanation for mismatches between X-ray and optical classifications of AGNs (Paolillo et al. 2004). Since the X-ray and optical observations of the sources in our sample were not obtained simultaneously, we need to consider this possibility. Yang et al. (2004) tested a subsample of CLASXS sources for flux variability. Of the 60 sources with  $4 \times 10^{-14} < f_{0.4-8 \text{ keV}} < 8 \times 10^{-14} \text{ erg cm}^{-2} \text{ s}^{-1}$ , 70% showed flux variability over a period of days to a year, depending on the location of the source. The change in spectral slope for 20% of these sources was sufficient to transform the X-ray spectral type from X-ray soft ( $\Gamma_{\text{eff}} \geq 1.2$ ) to X-ray hard ( $\Gamma_{\text{eff}} < 1.2$ ) or vice-versa. However, of the 60 sources tested for variability, only two are BLAGNs (CLASXS #293 and CLASXS #397), and neither of these exhibits sufficient spectral variability to change its X-ray spectral type. Of the 58 other sources tested for variability, two fall within our sample of non-BLAGNs with  $\Gamma_{\text{eff}} \geq 1.2$  (CLASXS #286 and CLASXS #199). CLASXS #286 does not exhibit sufficient spectral variability to change its X-ray spectral type, while CLASXS #199 does. We therefore conclude that while X-ray spectral variability does seem to be able to account for some of the X-ray unabsorbed ( $\Gamma_{\text{eff}} \geq 1.2$ ), optically obscured (non-BLAGN) sources, it is unlikely that it can account for the majority.

Silverman et al. (2005) argued that the broad emission lines for their X-ray unabsorbed, optically obscured sources were redshifted out of their optical spectral window. However, of the 84 X-ray unabsorbed, optically obscured sources in our spectroscopically observed 2–8 keV sample, all but one have at least one of the potentially broadened emission lines ( $\text{H}\alpha$ ,  $\text{H}\beta$ ,  $\text{MgII}$ ,  $\text{Ly}\alpha$ , or  $\text{CIV}$ ) measurable within the spectral window. Thus, this explanation also cannot account for the majority of our X-ray unabsorbed, optically obscured sources.

Moran et al. (2002) suggested that the light from the host galaxy may dilute the AGN signal. They found that 60% of their sample of local Seyfert 2s (i.e., HEX sources) would be classified as optically normal (i.e., as absorbers or star formers) if only the total emission were available (as would be the case for observations of high-redshift galaxies; see also Cardamone et al. 2007). Following this suggestion, Severgnini et al. (2003), Hasinger et al. (2005), and Garcet et al. (2007) posited that the absorbers and star formers in their sample were BLAGNs (rather than HEX sources) whose light was being diluted by the host galaxy light. However, the only possible evidence for this comes from one of the two sources in Severgnini et al. (2003). Severgnini et al. (2003) obtained improved optical spectroscopic observations of two X-ray unabsorbed, optically normal galaxies. Previous optical spectra for these sources did not cover the  $\text{H}\alpha$  line. As a result of the higher signal-to-noise and optimal wavelength coverage of new optical spectra they obtained, they found that the two X-ray unabsorbed sources exhibited strong and (possibly) broad  $\text{H}\alpha$ . They then simulated the effect of placing each source at a higher redshift using a template spectrum with both an AGN and a host galaxy component and concluded that for one of the sources, if it had instead been at  $z > 0.2$ , the  $\text{H}\alpha$  line would not have been visible due to dilution by the host galaxy light.

We stress that no evidence was presented by either Hasinger et al. (2005) or Garcet et al. (2007) to show

that their optically normal sources were diluted BLAGNs rather than diluted HEX sources. Furthermore, as discussed in the Introduction, Cowie et al. (2009) found that the non-BLAGNs in our OPTX sample with  $0.9 < z < 1.4$  are UV faint (as opposed to the BLAGNs, which are UV bright), indicating that we are not misclassifying as non-BLAGNs sources that are really BLAGNs. Similarly, Barger et al. (2005) argued against misclassification being a problem based on the weakness of the UV nuclei in the non-BLAGNs relative to their X-ray light. Thus, host galaxy dilution does not appear to be the explanation for the X-ray unabsorbed, optically normal sources in our sample.

Moreover, it does not seem likely that host galaxy dilution could cause BLAGNs to appear as HEX sources (i.e., wash out the broad lines while still allowing the narrow lines to be observed). The composite UV-optical spectrum for the sample of AGNs and quasars in the Large Bright Quasar Survey revealed that the equivalent widths of the broad lines is significantly greater than that of the narrow lines (Francis et al. 1991). In fact, in luminous QSOs there are often no narrow lines at all (Zheng et al. 1997). Thus, host galaxy dilution also does not appear to be the explanation for the X-ray unabsorbed, HEX sources in our sample.

## 6. CONCLUSIONS

We find that the observational problems discussed in Section 5 cannot explain most of the overlap that we see in the X-ray spectral properties for different optical spectral types. Until a better understanding is reached for how the X-ray and optical classifications relate to the obscuration of the central engine, the use of a mixed classification scheme can only complicate the interpretation of X-ray AGN samples. As a case in point, Cowie et al. (2009) found that a number of the BLAGNs in our OPTX sample have high ratios of ionizing flux to X-ray flux yet low values of  $\Gamma_{\text{eff}}$ . This suggests that there is not a one-to-one correspondence between the X-ray photon index and the opacity of the source, since any substantial neutral hydrogen opacity ( $N_H > 3 \times 10^{17} \text{ cm}^{-2}$ ) would absorb the ionizing flux, as Cowie et al. (2009) observed for the OPTX non-BLAGNs. Finally, we emphasize that any classification scheme which uses X-ray hardness ratio or, equivalently, effective photon index will be highly redshift dependent, which can introduce serious redshift bias. On the basis of this study, we advocate the adoption of a pure optical classification scheme for studying AGN with low signal-to-noise X-ray spectra. However if high quality X-ray spectra are available, they form an equally valid method of categorizing the objects (e.g. Winter et al. 2009).

L. T. was supported by a National Science Foundation Graduate Research Fellowship and a Wisconsin Space Grant Consortium Graduate Fellowship Award during portions of this work. We also gratefully acknowledge support from NSF grants AST 0407374 and AST 0709356 (L. L. C.) and AST 0239425 and AST 0708793 (A. J. B.), the University of Wisconsin Research Committee with funds granted by the Wisconsin Alumni Research Foundation and the David and Lucile Packard Foundation (A. J. B.). A. J. B. thanks the Aspen Center for Physics

for hospitality during the completion of this work. This article is part of L. T.'s Ph.D. thesis work at the Univer-

sity of Wisconsin-Madison.

## REFERENCES

- Akiyama, M., et al., 2000, *ApJ*, 532, 700  
Akiyama, M., Ueda, Y., Ohta, K., Takahashi, T., & Yamada, T. 2003, *ApJS*, 148, 275  
Akylas, A., Georgantopoulos, I., Georgakakis, A., Kitsionas, S., & Hatziminaoglou, E. 2006, *A&A*, 459, 693  
Alexander, D. M., Aussel, H., Bauer, F. E., Brandt, W. N., Hornschemeier, A. E., Vignali, C., Garmire, G. P., & Schneider, D. P. 2002, *ApJ*, 568, L85  
Alexander, D. M., et al., 2003, *AJ*, 126, 539  
Antonucci, R. 1993, *ARA&A*, 31, 473  
Barcons, X., Carrera, F. J., & Ceballos, M. T. 2003, *MNRAS*, 339, 757  
Barger, A. J., Cowie, L. L., Brandt, W. N., Capak, P., Garmire, G. P., Hornschemeier, A. E., Steffen, A. T., & Wehner, E. H. 2002, *AJ*, 124, 1839  
Barger, A. J., et al., 2003, *AJ*, 126, 632  
Barger, A. J., Cowie, L. L., Mushotzky, R. F., Yang, Y., Wang, W.-H., Steffen, A. T., & Capak, P. 2005, *AJ*, 129, 578  
Barger, A. J., Cowie, L. L., Steffen, A. T., Hornschemeier, A. E., Brandt, W. N., & Garmire, G. P. 2001, *ApJ*, 560, L23  
Bauer, F. E., Alexander, D. M., Brandt, W. N., Hornschemeier, A. E., Vignali, C., Garmire, G. P., & Schneider, D. P. 2002, *AJ*, 124, 2351  
Beckmann, V., Soldi, S., Shrader, C. R., Gehrels, N., & Product, N. 2006, *ApJ*, 652, 126  
Brandt, W. N., et al., 2001, *AJ*, 122, 2810  
Brusa, M., et al., 2003, *A&A*, 409, 65  
Caccianiga, A., et al., 2004, *A&A*, 416, 901  
Cardamone, C. N., Moran, E. C., & Kay, L. E. 2007, *AJ*, 134, 1263  
Comastri, A., Fiore, F., Vignali, C., Matt, G., Perola, G. C., & La Franca, F. 2001, *MNRAS*, 327, 781  
Corral, A., Barcons, X., Carrera, F. J., Ceballos, M. T., & Mateos, S. 2005, *A&A*, 431, 97  
Cowie, L. L., Barger, A. J., & Trouille, L. 2009, *ApJ*, 692, 1476  
Della Ceca, R., et al., 2008, *A&A*, 487, 119  
Elvis, M., et al., 2009, *ArXiv e-prints*  
Faber, S. M., et al., 2003, *Proc. SPIE*, 4841, 1657  
Fiore, F., et al., 2003, *A&A*, 409, 79  
Francis, P. J., Hewett, P. C., Foltz, C. B., Chaffee, F. H., Weymann, R. J., & Morris, S. L. 1991, *ApJ*, 373, 465  
Gallagher, S. C., Brandt, W. N., Chartas, G., Priddey, R., Garmire, G. P., & Sambruna, R. M. 2006, *ApJ*, 644, 709  
Garcet, O., et al., 2007, *A&A*, 474, 473  
Gehrels, N. 1986, *ApJ*, 303, 336  
Georgantopoulos, I. & Zezas, A. 2003, *ApJ*, 594, 704  
Giacconi, R., et al., 2002, *ApJS*, 139, 369  
Gialisco, M., et al., 2004, *ApJ*, 600, L93  
Hall, P. B., Gallagher, S. C., Richards, G. T., Alexander, D. M., Anderson, S. F., Bauer, F., Brandt, W. N., & Schneider, D. P. 2006, *AJ*, 132, 1977  
Harrison, F. A., Eckart, M. E., Mao, P. H., Helfand, D. J., & Stern, D. 2003, *ApJ*, 596, 944  
Hasinger, G. 2008, *A&A*, 490, 905  
Hasinger, G., Miyaji, T., & Schmidt, M. 2005, *A&A*, 441, 417  
Hornschemeier, A. E., et al., 2001, *ApJ*, 554, 742  
Kim, M., et al., 2007a, *ApJS*, 169, 401  
Kim, M., et al., 2007b, *ApJ*, 659, 29  
Kuraszkiewicz, J., et al., 2009a, *ApJ*, 692, 1143  
Kuraszkiewicz, J., Wilkes, B. J., Schmidt, G., Smith, P. S., Cutri, R., & Czerny, B. 2009b, *ApJ*, 692, 1180  
La Franca, F., et al., 2005, *ApJ*, 635, 864  
Laird, E. S., et al., 2009, *ApJS*, 180, 102  
Lawrence, A. & Elvis, M. 1982, *ApJ*, 256, 410  
Lehmer, B. D., et al., 2005, *ApJS*, 161, 21  
Lockman, F. J., Jahoda, K., & McCammon, D. 1986, *ApJ*, 302, 432  
Luo, B., et al., 2008, *ApJS*, 179, 19  
Maccaro, T., Gioia, I. M., Wolter, A., Zamorani, G., & Stocke, J. T. 1988, *ApJ*, 326, 680  
Maiolino, R., Marconi, A., Salvati, M., Risaliti, G., Severgnini, P., Oliva, E., La Franca, F., & Vanzani, L. 2001, *A&A*, 365, 28  
Martin, D. C., et al., 2005, *ApJ*, 619, L1  
Mateos, S., Barcons, X., Carrera, F. J., Ceballos, M. T., Hasinger, G., Lehmann, I., Fabian, A. C., & Streblyanska, A. 2005, *A&A*, 444, 79  
Moran, E. C., Filippenko, A. V., & Chornock, R. 2002, *ApJ*, 579, L71  
Mushotzky, R. F. 1984, *Proceedings of IAU/COSPAR Meeting on High Energy Astrophysics and Cosmology*, Rogen, Bulgaria, *Adv. Space Research*, 34, 157  
Mushotzky, R. F., Cowie, L. L., Barger, A. J., & Arnaud, K. A. 2000, *Nature*, 404, 459  
Nandra, K., et al., 2005, *MNRAS*, 356, 568  
Panessa, F. & Bassani, L. 2002, *A&A*, 394, 435  
Paolillo, M., Schreier, E. J., Giacconi, R., Koekemoer, A. M., & Grogin, N. A. 2004, *ApJ*, 611, 93  
Pappa, A., Georgantopoulos, I., Stewart, G. C., & Zezas, A. L. 2001, *MNRAS*, 326, 995  
Sazonov, S., Revnivtsev, M., Krivonos, R., Churazov, E., & Sunyaev, R. 2007, *A&A*, 462, 57  
Schmidt, M., et al., 1998, *A&A*, 329, 495  
Severgnini, P., et al., 2003, *A&A*, 406, 483  
Silverman, J. D., et al., 2005, *ApJ*, 618, 123  
Silverman, J. D., et al., 2008, *ApJ*, 679, 118  
Simpson, C. 2005, *MNRAS*, 360, 565  
Stark, A. A., Gammie, C. F., Wilson, R. W., Bally, J., Linke, R. A., Heiles, C., & Hurwitz, M. 1992, *ApJS*, 79, 77  
Steffen, A. T., Barger, A. J., Capak, P., Cowie, L. L., Mushotzky, R. F., & Yang, Y. 2004, *AJ*, 128, 1483  
Steffen, A. T., Barger, A. J., Cowie, L. L., Mushotzky, R. F., & Yang, Y. 2003, *ApJ*, 596, L23  
Szokoly, G. P., et al., 2004, *ApJS*, 155, 271  
Tajer, M., et al., 2007, *A&A*, 467, 73  
Tozzi, P., et al., 2006, *A&A*, 451, 457  
Trouille, L., Barger, A. J., Cowie, L. L., Yang, Y., & Mushotzky, R. F. 2008, *ApJS*, 179, 1  
Tueller, J., Mushotzky, R. F., Barthelmy, S., Cannizzo, J. K., Gehrels, N., Markwardt, C. B., Skinner, G. K., & Winter, L. M. 2008, *ApJ*, 681, 113  
Ueda, Y., Akiyama, M., Ohta, K., & Miyaji, T. 2003, *ApJ*, 598, 886  
Virani, S. N., Treister, E., Urry, C. M., & Gawiser, E. 2006, *AJ*, 131, 2373  
Wang, W.-H., Cowie, L. L., & Barger, A. J. 2006, *ApJ*, 647, 74  
Wilkes, B. J., Schmidt, G. D., Cutri, R. M., Ghosh, H., Hines, D. C., Nelson, B., & Smith, P. S. 2002, *ApJ*, 564, L65  
Winter, L. M., Mushotzky, R. F., Reynolds, C. S., & Tueller, J. 2009, *ApJ*, 690, 1322  
Winter, L. M., Mushotzky, R. F., Tueller, J., & Markwardt, C. 2008, *ApJ*, 674, 686  
Wolter, A., Gioia, I. M., Henry, J. P., & Mullis, C. R. 2005, *A&A*, 444, 165  
Yang, Y., Mushotzky, R. F., Steffen, A. T., Barger, A. J., & Cowie, L. L. 2004, *AJ*, 128, 1501  
Yenko, B., Barger, A. J., Trouille, L., & Winter, L. M. 2009, *ApJ*, 698, 380  
Zamorani, G., et al., 1981, *ApJ*, 245, 357  
Zheng, W., Kriss, G. A., Telfer, R. C., Grimes, J. P., & Davidsen, A. F. 1997, *ApJ*, 475, 469